Interaction of Gold Nanoparticles in Barium Titanate Thin Films

Yaodong Yang,* Jianjun Yao, Yu U. Wang, Jiefang Li, Jaydip Das, and Dwight Viehland

Department of Materials Science and Engineering, Virginia Tech, Blacksburg, Virginia 24061

ARTICLE

ABSTRACT A novel approach to control the grain size of oxide thin film materials has been investigated. Perovskite $BaTiO_3$ shows interesting grain structures when deposited on gold predeposited, (111)-oriented, single-crystal $SrTiO_3$ substrates. Solid oxide films grow epitaxially on patterned seed layers and show variations in grain size relative to the films deposited on $SrTiO_3$ directly.

KEYWORDS: nanoparticle · thin film · interaction between metal and ceramic · piezoelectricity · pulsed laser deposition

Piezoelectric oxide materials have drawn recent research interest due to their potential in many applications ranging from sensors to radio frequency devices.[1−3] The piezoelectric properties depend on the polarization distribution of individual domains, which is affected by grain size and orientation.[4−6] Growth of piezoelectric thin films on particular substrates can enhance the utility of these materials for practical purposes due to the possibility for size and cost reduction, better compatibility, and improved device performance.[1] Recent developments in thin film technologies offer the opportunity to control the grain size and distribution precisely and to perform a detailed study of the dependence of the piezoelectric response on grain structures. For practical on-chip applications, such films can be useful either as a continuous film or with well-defined patterns. Patterns also can be made by, for example, focused ion beam which involves a tedious and expensive process.

Consider perovskite $BaTiO_3$ (BTO) thin films, for example, that exhibit good piezoelectric responses.[7−9] Epitaxial BTO films can be deposited by pulsed laser deposition (PLD) at a temperature of about 700 °C or higher. To make BTO nanostructures, one has to pattern the film layer postdeposition because the deposition temperature is too high for a polymer photoresist as normally used in lithography techniques.

Here, we report a simple technique to pattern the BTO films directly during deposition on gold (Au) nanoparticle predeposited $SrTiO_3$ (STO) substrates. The predeposited Au served as a seed layer that affects the growth mechanism of the BTO layer.[10] The BTO grain size and shape are found to depend on the Au nanoparticles. Note that, in addition to work as a patterned template, Au might be used for other purposes. For example, Au being a well-known electrode material can serve as embedded electrodes to apply electric voltage across the piezoelectric materials. Further, the Au−BTO can be considered as a metal−ceramic composite, and it might be possible to study the interaction between metal and ceramic that can help us bring these advantages from each material to achieve a better performance.[11]

RESULTS AND DISCUSSION

Figure 1 illustrates the SEM results. Parts a and b show images for the patterned BTO films with Au predeposited seed layer. Panels c−e show images for BTO films deposited directly on the STO substrate with an attached TEM grid. From Figure 1a, we can clearly see that the BTO films have a hexagonal shaped pattern. These patterns look exactly similar to the patterns in the TEM grid through which the Au was sputtered. This indicates that the grid with hexagonal shaped windows first helps to pattern the Au layer, and then the Au layer works as a positive template to pass this pattern to the BTO layer by controlling the grain distribution.

To study the boundary in more detail, we obtained SEM images of the positive/negative patterned area (marked by a dot

*Address correspondence to yaodongy@vt.edu.

Received for review July 21, 2009 and accepted September 02, 2009.

Published online September 16, 2009.
10.1021/nn9008406 CCC: $40.75

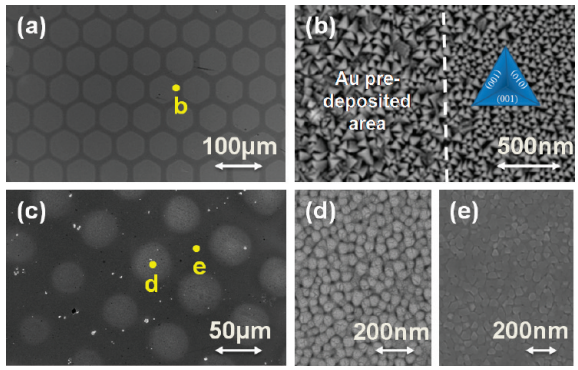

Figure 1. SEM images of (a) patterned Au predeposited BTO; (b) higher magnification image of the boundary area as marked in (a), where the left side is Au predeposited and patterned area; (c) directly patterned BTO thin film on STO substrate; and (d,e) higher magnification images of grid uncovered and covered areas as marked in (c).

"b" in Figure 1a), as shown in Figure 1b. A dashed line is used to illustrate this boundary. A notable difference between the Au predeposited areas can be found: the grain size in the positive patterned (*i.e.*, Au predeposited) area was approximately 100 nm, whereas that in the negative patterned (STO exposed) area was approximately 50 nm. Furthermore, one can see that both areas have pyramidal grain morphologies that are indicative of (111)-oriented BTO grains. A schematic diagram in Figure 1b illustrates the BTO unit cell projected onto the (111) plane, representing the pyramidal shape.

Next, we obtained images of the BTO morphology when deposited directly on STO without a Au seed layer as a control sample. In this case, we put the copper grid in the chamber and deposited BTO directly onto the STO substrate through it. From Figure 1c, it can clearly be seen that the BTO film morphology appears circular instead of hexagonal, and that there was no clear boundary that developed. We also obtained images under higher magnification of both uncovered and covered areas, as shown in Figure 1d,e. Both areas had BTO films, and the difference was that there was more BTO in the uncovered window areas. Note that the grain size and shape are nearly the same for both areas. We also noticed a slight difference between the right-hand side of Figure 1b and Figure 1d: the triangular grains in Figure 1b are sharper than that in Figure 1d, even though the grains are the same size. This difference may have resulted from the presence of some Au deposition beneath the masked areas at the boundary. Small Au particles could affect the BTO grain growth after dewetting.

On the basis of the above results, it looks like the Au seed layer seemed to play an important role in affecting the grain growth in the BTO layer. In order to understand the effect of the Au seed layer on the BTO growth mechanism better, we prepared a series of control samples. Figure 2a shows BTO films deposited directly on STO substrate (without Au seed layer) under the same conditions, as mentioned above. Part b shows a SEM image taken from an as-prepared Au layer deposited by argon sputtering at room temperature for 20 s. This layer looks more or less continuous with several randomly distributed holes that are tens of nanometers in size. Part c is an image showing "hundreds of nanometer large" Au islands obtained after annealing at 750 °C for 40 min in a vacuum chamber at an oxygen pressure of 100 mTorr. Since this is a control experiment, the annealing process was performed in the same manner as the PLD deposition procedure, but without turning on the laser. From the image, we can see numerous island-like formations that are somewhat regularly spaced: some of which are circular in shape and others which are trilateral in shape. This island-like formation in Au on the STO substrate can be attributed to the difference in the surface energies and diffusion kinetics between the metal (Au) and oxide (STO) and the growth and coalescence of Au particle at such annealing temperatures.[12] Part d shows the PLD-deposited BTO film morphology on the Au seeded STO substrate, which had larger grain sizes than the BTO film grown directly on STO (see Figure 2a). The findings for this control experiment in Figure 2 clearly demonstrate that the Au seed islands on the STO substrate help to grow the BTO grains faster, resulting in larger grains than the BTO grown directly on the STO substrate.

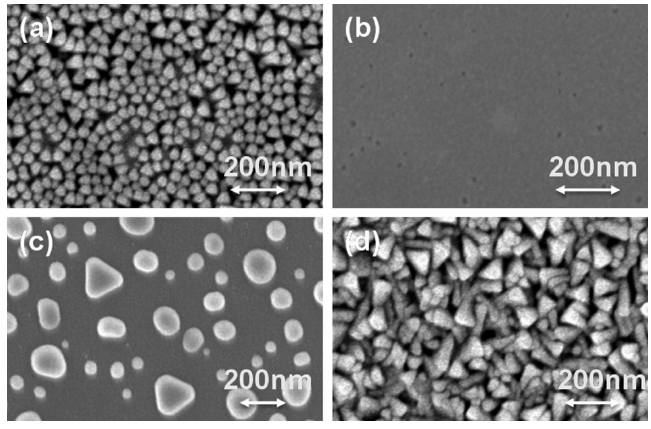

Figure 2. SEM images of (a) BTO thin film deposited directly onto a (111)-oriented STO substrate by PLD; (b) Au film deposited by sputtering for 20 s at room temperature; (c) same sample shown in (b) after annealing at 750 °C for 40 min; and (d) BTO thin film with Au predeposited layer showing larger grain sizes than when grown directly on STO (see panel a).

We then used FIB to lift out a small cross-sectional piece as a TEM sample. HRTEM images in Figure 3 provide more detailed information concerning the morphology and grain size of the BTO structure that was grown on the Au predeposited substrate. Figure 3a shows the Au nanoparticles and the BTO grains. One can see that the Au formed nanoparticles of two different sizes: the dominant one was approximately 40−50 nm in size and

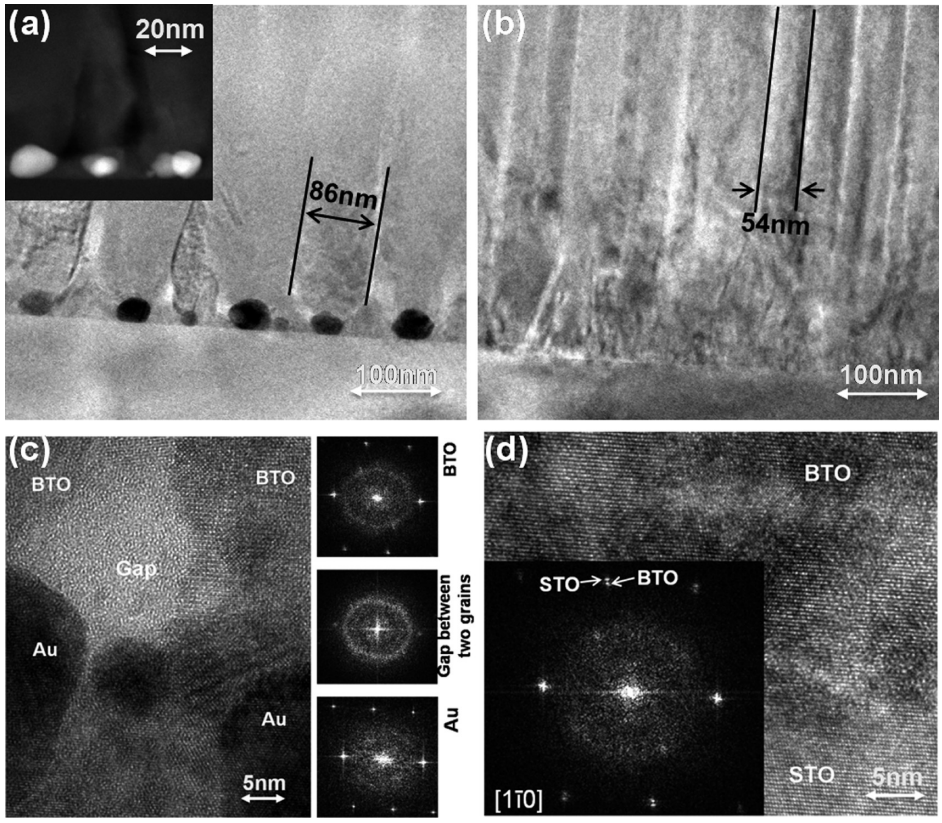

Figure 3. TEM images (a,b) and HRTEM images (c,d) of BTO thin film to reveal the interphase interfacial areas with (a,c) and without (b,d) Au seed layer, respectively. Inset in (a) is a STEM image taken from the same area as that of the TEM image; insets in (c) are power spectra taken from Au, gap, and BTO areas, respectively, where the corresponding areas from which these spectra were taken are marked in the TEM image, and the zone axis is the same. Inset in (d) is a power spectrum taken from the entire area shown in the image.

was distributed more or less in a regular fashion, and the minor one was approximately 15 nm in size and was occasionally observed in the space between major particles. This indicates that the hexagonal shaped Au layer internally breaks up into near regularly spaced Au islands, possibly on heating the substrate.[10,13] From the image, we can also see that the BTO nucleated and grew from the dominant Au nanoparticles, where each metal nanoparticle supports one BTO columnar grain: the regularity of the Au nanoparticle spacing seemed to be passed onto the BTO columns. Two lines are drawn in the image to serve as a guide for the eyes to follow the BTO columnar grains grown on Au nanoparticles. The inset scanning TEM (STEM) image shows that there are notable gaps between the BTO grains.

Figure 3b shows a HRTEM of the BTO film that was deposited directly on a STO substrate without seed layer. Again, one can see columnar grain growth, as marked by two lines in the image. There were two noticeable differences between the images in Figure 3a and 3b. First, the BTO grain size (the lateral distance between the lines) was about 90 nm for the Au predeposited film (as determined by the distance between Au nanoparticles), whereas for the areas without any Au beneath, it was about 50 nm. This is in agreement with the SEM images shown in Figure 1. Second, the BTO−STO interfacial area for the film grown with Au was more ordered than that for the other film. The BTO grain boundaries are quite visible just above the Au nanoparticle in Figure 3a, while in Figure 3b, the BTO columnar grains could be clearly seen at only about 100 nm above the substrate surface. This demonstrates that the Au nanoparticles significantly reduce the interfacial stress in the BTO and thus help to relax the lattice distortion in BTO much faster. Elemental analysis by EDS (attached to the Titan HRTEM system) confirmed that the areas discussed above were indeed BTO and Au (Figure S1 in the Supporting Information).

Figure 3c shows a higher magnification image of the grain boundary of Figure 3a. It can be seen that the BTO grains grown on the Au nanoparticles are single crystalline, which is marked by "BTO" in the image, as determined by power spectra to have the same orientation as the STO substrate. Between two oriented BTO grains, there was a small transition area that corresponded to an amorphous phase, which is marked as "gap" in the image. The Au nanoparticles were crystalline as evidenced by power spectra. Clearly, the BTO columnar grains nucleated and grew from the crystalline gold nanoparticles in an orderly manner. However, a close look at the interphase interface of

the BTO film shows that BTO is reasonably epitaxial with the STO substrate, as shown in Figure 3d. The inset shows spot splitting in a power spectrum, which proves epitaxial growth from the STO.

The SEM and TEM images shown in Figures 2 and 3, respectively, indicate that Au layers serve as nucleation sites for the formation of BTO grains. As evident from the images, without the Au layer, the BTO interfacial region is notably stressed. This compressive stress presumably comes from the 2.5% lattice mismatch between the BTO film and the STO substrate. The BTO nuclei crystallize on the STO substrate and subsequently merge together during grain growth. To minimize interfacial energy between grains and the substrate, grains grow into a columnar morphology with increasing thickness. For BTO films deposited directly on STO substrates, elastic stress is relaxed with columnar grain growth, producing quite regular interfaces between BTO grains at film thickness above about 100 nm.

For the case of Au predeposited BTO, the growth process is more complicated. The lattice parameter for cubic Au is about $a = 4.07$ Å, while for STO, it is about $a = 3.90$ Å. BTO is tetragonal, with lattice parameters of $(a_t, c_t) = (3.99$ Å, 4.01 Å). Interestingly, the lattice parameters of BTO lie between those of Au and STO, which is a little closer to that of Au; thus using STO−Au as a substrate will match the BTO lattice parameter better than only STO or Au substrates. Figure 3c shows that Au is epitaxial with the STO substrate, which would reduce the lattice parameter of Au nanoparticles by epitaxial stress to become even closer to that of BTO. This may be a reason for preferred BTO nucleation on Au nanoparticles, which helps to relax the stress imposed on BTO from the STO substrate. Accordingly, this would provide a way for better epitaxy, and the lattice mismatch is accommodated by the amorphous areas between BTO grains in the vicinity of Au nanoparticles. As a result, BTO grain boundaries are well formed at a much smaller distance from the substrate surface. From Figure 3a,c, it can clearly be seen that ordered BTO grains grow directly from the Au nanoparticles, and that the grain size is determined by the distance between nucleation sites (*i.e.*, Au nanoparticles). In the regions between Au nanoparticles with exposed STO substrate surface, a triangular shaped small gap region of amorphous BTO existed that reduced the interfacial stress between gold, BTO, and STO. As the array of BTO grains on Au nanoparticles began to grow longer, this gap area was closed, leaving only a residual triangular amorphous region at the interfaces where all three phases were in close proximity, as shown in Figure 3a.

PFM was then used to investigate the ferroelectric domain structures in the Au predeposited BTO thin films in order to study the effect of grain size on the physical properties. For this purpose, the Au buffer layer and BTO film were deposited on conducting Nb (0.5 wt %) doped STO substrates, which serve as the bottom electrode for the PFM measurements. The topographic AFM image is shown in Figure 4a, and the corresponding piezoresponse amplitude and phase images are listed in panels b and c. As shown in Figure 4a−c, the surface morphology and piezoresponse image were composed of two regions, indicated by white lines. The left side was smoother than the right side (Au predeposited) and had a lower degree of roughness and smaller grain size. The difference in height between these two regions was approximately 60 nm, indicating that BTO grains grow faster on Au nanoparticles, which also supports our observations from SEM and TEM images. The PR amplitude data are shown in bigger and darker triangles to indicate stronger piezoresponses, and PR phase signal is shown in darker colors to better reveal areas with stronger piezoresponses, as shown in Figure 4b,c. This image shows that the PR signal (both phase and amplitude) on the left side does not have significant contrast, indicating that the film is not strongly piezoelectric. However,

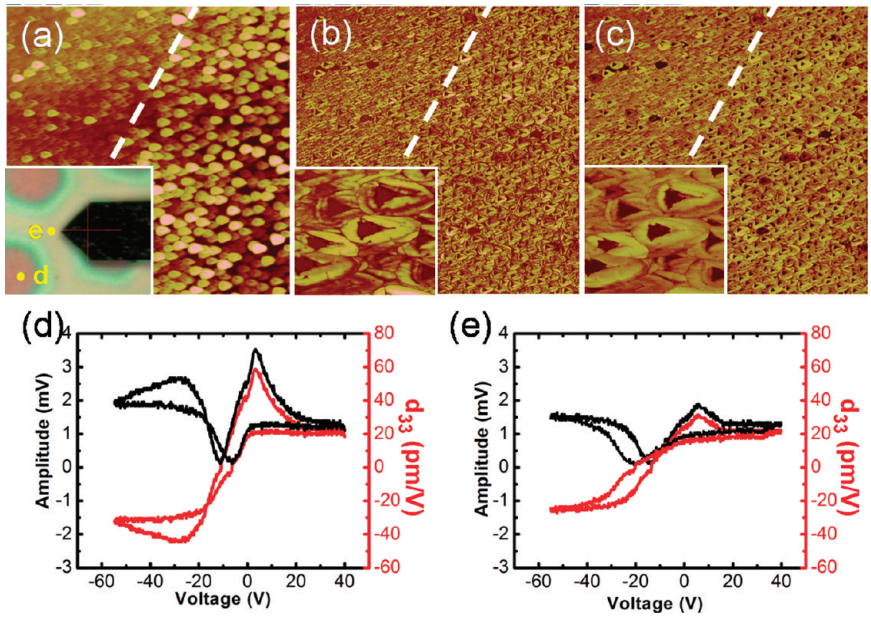

Figure 4. AFM and PFM study of transition zone: (a) AFM topography image of an area of 20 μm × 20 μm, where the inset is an optical view of the scanned area; (b,c) corresponding piezoresponse amplitude image and piezoresponse phase image, where the insets are the enlarged image of the area (1.8 μm × 1.8 μm) with several triangular grains grown on Au predeposited STO; and (d,e) local piezoelectric hysteresis loops measured in and out of Au predeposited areas (marked by "d" and "e" as in Figure 4a inset), respectively.

on the right side of this image, the triangular BTO grains show pronounced contrast, especially at the top of the triangles. The size and density of dark regions on the right side of the image were both greater than on the left. The inset of Figure 4b,c enlarges several grains. In this inset, we can see that the piezoresponse also had a uniform triangular shape, indicating that the PR in one triangular grain is from a single domain. These PFM images show that the domain distribution of films grown on Au predeposited areas is much more like a single-domain, single-crystal state than the areas grown directly on STO.

In order to get a better insight into the local piezoelectric properties of the two different regions, piezoelectric hysteresis loops were measured under the same AC bias conditions (3 V, 20 kHz). The measurement used a conductive cobalt-coated cantilever with a spring constant of 0.0678 N/m. The results can be seen in Figure 4d,e. A voltage shift of the loops toward a negative bias was found: this kind of shift has been attributed to the formation of space charges at the film/electrode interface.[14] The coercive voltage of the Au predeposited area (5 V) was a little smaller than the other region (8 V). An asymmetric shape for the loops was observed, which may have resulted from higher polarization under positive bias.[15] Meanwhile, the average amplitude of the Au predeposited area and corresponding piezoelectric coefficient was also greater than that of the other regions. The magnitude of d_{33} in the Au predeposited area (red line in Figure 4d) reached up to 60 pm/V; however, out of the Au predeposited areas, the peak value was about 30 pm/V (marked by the red line in Figure 4e). This indicates that the Au predeposited area with larger grain sizes at the nanoscale has better piezoelectric properties. We believe that the increase of grain boundary area on the region without Au might degrade the piezoelectric properties of the BTO film.

CONCLUSIONS

In summary, Au nanoparticles have been shown to be capable of controlling the grain size of BTO films, without change in the epitaxial growth conditions of the thin films. These findings should allow for enabling control of piezoelectric properties *via* domain engineering. Since Au nanoparticles show ferromagnetism for particle sizes smaller than 10 nm,[16−18] these findings also establish a relationship between BTO and Au, which may allow for novel magnetoelectric interactions.

METHODS

In this investigation, we used a transmission electron microscopy (TEM) grid (300 mesh copper grid from SPI company) with hexagonal windows as a template to sputter Au thin layers onto (111)-oriented STO single-crystal substrates at room temperature for 20 s. The current used to sputter argon was 45 mA. The TEM grid was subsequently removed. A pulsed laser deposition (PLD) system with a KrF laser of wavelength 248 nm (Lambda Physik 305i) was used to deposit a BTO film on the patterned Au predeposited STO substrate. Deposition was done in a vacuum chamber at an oxygen pressure of 100 mTorr. The distance between the substrate and target was 8 cm, and the substrate was heated to 750 °C. A laser spot of 3 mm^2 size and 1.2 J/cm^2 energy density was rastered at a frequency of 10 Hz on a stoichiometric target surface for 40 min. After deposition, the films were cooled under a 760 Torr oxygen pressure to room temperature. For comparison purposes, we attached the same TEM grid to the STO substrate and directly deposited BTO films on the STO substrate at the same temperature.

Scanning electron microscopy (SEM) images and energy-dispersive spectra (EDS) were obtained using a LEO (Zeiss) 1550 high-performance Schottky field-emission SEM. A FEI Helios 600 NanoLab FIB SEM was used to prepare and lift-out TEM samples. A FEI Titan 300 high-resolution TEM (HRTEM) was used to obtain lattice images and high-resolution EDS. Atomic force (AFM) and piezoelectric force (PFM) microscopy images were obtained by a Veeco Dimension 3100 Nanoman AFM.

Acknowledgment. Support for this work was provided by the Division of Materials Research of the National Science Foundation. Authors also give thanks for NCFL in Virginia Tech for all the SEM, FIB, and TEM support.

Supporting Information Available: Elemental analysis by EDS (attached to the Titan HRTEM system). This material is available free of charge *via* the Internet at http://pubs.acs.org.

REFERENCES AND NOTES

1. Nan, C. W.; Bichurin, M. I.; Dong, S. X.; Viehland, D.; Srinivasan, G. Multiferroic Magnetoelectric Composites: Historical Perspective, Status, and Future Directions. *J. Appl. Phys.* **2008**, *103*, 031101-35.
2. Ryu, J.; Priya, S.; Uchino, K.; Kim, H. E. Magnetoelectric Effect in Composites of Magnetostrictive and Piezoelectric Materials. *J. Electroceram.* **2002**, *8*, 107–119.
3. Yang, Y. D.; Priya, S.; Wang, Y. U.; Li, J. F.; Viehland, D. Solid-State Synthesis of Perovskite-Spinel Nanocomposites. *J. Mater. Chem.* **2009**, *19*, 4998–5002.
4. Shao, S. F.; Zhang, J. L.; Zhang, Z.; Zheng, P.; Zhao, M. L.; Li, J. C.; Wang, C. L. High Piezoelectric Properties and Domain Configuration in Batio3 Ceramics Obtained through the Solid-State Reaction Route. *J. Phys. D: Appl. Phys.* **2008**, *41*, 125408–125413.
5. Islam, R. A.; Priya, S. Effect of Piezoelectric Grain Size on Magnetoelectric Coefficient of $Pb(Zr_{0.52}Ti_{0.48})O$-3-$Ni_{0.8}Zn_{0.2}Fe_2O_4$ Particulate Composites. *J. Mater. Sci.* **2008**, *43*, 3560–3568.
6. Buhlmann, S.; Dwir, B.; Baborowski, J.; Muralt, P. Size Effect in Mesoscopic Epitaxial Ferroelectric Structures: Increase of Piezoelectric Response with Decreasing Feature Size. *Appl. Phys. Lett.* **2002**, *80*, 3195–3197.
7. Zheng, H.; Wang, J.; Lofland, S. E.; Ma, Z.; Mohaddes-Ardabili, L.; Zhao, T.; Salamanca-Riba, L.; Shinde, S. R.; Ogale, S. B.; Bai, F.; *et al.* Multiferroic $BaTiO_3$-$CoFe_2O_4$ Nanostructures. *Science* **2004**, *303*, 661–663.
8. Hlinka, J.; Ondrejkovic, P.; Marton, P. The Piezoelectric Response of Nanotwinned $BaTiO_3$. *Nanotechnology* **2009**, *20*, 105709–105716.
9. Vijatovic, M. M.; Bobic, J. D.; Stojanovic, B. A. History and Challenges of Barium Titanate: Part I. *Sci. Sinter.* **2008**, *40*, 155–165.
10. Sun, X. N.; Felicissimo, M. P.; Rudolf, P.; Silly, F. Nacl Multi-Layer Islands Grown on Au(111)-(22 × Root 3) Probed by Scanning Tunneling Microscopy. *Nanotechnology* **2008**, *19*, 495307-5.

11. Yang, Y. D.; Qu, L. T.; Dai, L. M.; Kang, T. S.; Durstock, M. Electrophoresis Coating of Titanium Dioxide on Aligned Carbon Nanotubes for Controlled Syntheses of Photoelectronic Nanomaterials. *Adv. Mater.* **2007**, *19*, 1239–1243.
12. Silly, F.; Castell, M. R. Bimodal Growth of Au on $SrTiO_3$(001). *Phys. Rev. Lett.* **2006**, *96*, 086104-4.
13. Donohoe, A. J.; Robins, J. L. Nucleation Kinetics of Silver Deposited onto UHV Cleaved Surfaces of NaCl, KCl and KBr. *Thin Solid Films* **1976**, *33*, 363–372.
14. Gruverman, A.; Kholkin, A.; Kingon, A.; Tokumoto, H. Asymmetric Nanoscale Switching in Ferroelectric Thin Films by Scanning Force Microscopy. *Appl. Phys. Lett.* **2001**, *78*, 2751–2753.
15. Hong, J.; Song, H. W.; Lee, H. C.; Lee, W. J.; No, K. Structure and Electrical Properties of Pb(ZrxTi1-X)O-3 Deposited on Textured Pt Thin Films. *J. Appl. Phys.* **2001**, *90*, 1962–1967.
16. Crespo, P.; Litran, R.; Rojas, T. C.; Multigner, M.; de la Fuente, J. M.; Sanchez-Lopez, J. C.; Garcia, M. A.; Hernando, A.; Penades, S.; Fernandez, A. Permanent Magnetism, Magnetic Anisotropy, and Hysteresis of Thiol-Capped Gold Nanoparticles. *Phys. Rev. Lett.* **2004**, *93*, 087204-8.
17. Dutta, P.; Pal, S.; Seehra, M. S.; Anand, M.; Roberts, C. B. Magnetism in Dodecanethiol-Capped Gold Nanoparticles: Role of Size and Capping Agent. *Appl. Phys. Lett.* **2007**, *90*, 213102-5.
18. Luo, W.; Pennycook, S. J.; Pantelides, S. T. S-Electron Ferromagnetism on Gold and Silver Nanoclusters. *Nano Lett.* **2007**, *7*, 3134–3137.